L/S-Band Frequency Reconfigurable Multiscale Phased Array Antenna With Wide Angle Scanning

Haider, Nadia; Yarovoy, Alexander G.; Roederer, Antoine G.

DOI
10.1109/TAP.2017.2722685

Publication date
2017

Document Version
Accepted author manuscript

Published in
IEEE Transactions on Antennas and Propagation

Citation (APA)
Haider, N., Yarovoy, A. G., & Roederer, A. G. (2017). L/S-Band Frequency Reconfigurable Multiscale Phased Array Antenna With Wide Angle Scanning. *IEEE Transactions on Antennas and Propagation*, *65*(9), 4519-4528. https://doi.org/10.1109/TAP.2017.2722685

L/S-Band Frequency Reconfigurable Multi-Scale Phased Array Antenna with Wide Angle Scanning

Nadia Haider, Alexander G. Yarovoy, *Fellow, IEEE* and Antoine G. Roederer, *Life Fellow, IEEE*

***Abstract*—A frequency reconfigurable phased array element is presented. The operational band of the single port L/S-band antenna can be selected by modifying the element apertures with p-I-n diode switches. The antenna element satisfies strict requirements on its frequency band separation (2.2:1), size, feeding structure and control lines to be integrated into a phased array system. A multi-scale array topology is proposed to achieve wide angle scanning (±60°) in both operational bands of the array.**

***Index Terms*— Frequency reconfiguration; planar antenna; phased array; wide angle scanning.**

I. INTRODUCTION

SENSORS such as phased array radars play a crucial role for surveillance, threat identification and post-disaster management. However, different scenarios impose extremely diverse system requirements. Phased array systems occupy a large area, when separate apertures are used for each function. For ships and aircrafts, space and weight are at a premium and reconfigurable multi-band antennas are very attractive solutions for future multi-function sensors.

Reconfiguration using RF-switches has been proposed for various purposes [1-13] but rarely for array applications. Furthermore, the frequency ranges of these reconfigurable antennas are not sufficient to cover multiple radar bands with frequency ratios over an octave. In this work a frequency reconfigurable element for active phased array radars is designed based on an adaptive antenna-aperture concept. The proposed concept involves geometrical reconfiguration of each radiating cell of a phased array by the use of RF-switches. The distinctive properties of the approach are its array compatibility, large separation of the bands (2.2:1) and well defined radiation and circuital characteristics in both bands.

For dual-band wide angle scanning, a small element periodicity is vital and, to avoid grating lobes at the higher frequencies, the elements need to be placed very densely at the lower frequency. As a result, coupling increases and reduces the radiation efficiency and the gain. Hence, there is a clear trade-off between the maximum scan volume at the high frequency and the coupling in the low frequency band. For large separation between the bands, reconfigurability is required at antenna element and at array topology level to adapt the array. Only a very limited number of reconfigurable or dual-band antennas have been designed for array applications in the last decades [14-24]. To date examples of multi-band antenna arrays with both a frequency ratio beyond 2:1 and 2-D scanning capability of more than ±45° in both bands are very limited in open literature [25-27]. In this work, a multi-scale array structure is introduced providing wide angle scanning in both L- and S-band. The advantage of this novel configuration is twofold: reduced mutual coupling in the lower band, and increased scanning volume for the higher band [28]. A planar array demonstrator validated the proposed concept.

This paper is organized in four sections. In Section II the design and experimental verification of the frequency reconfigurable antenna element are presented. Section III details the multi-scale array concept, the planar array

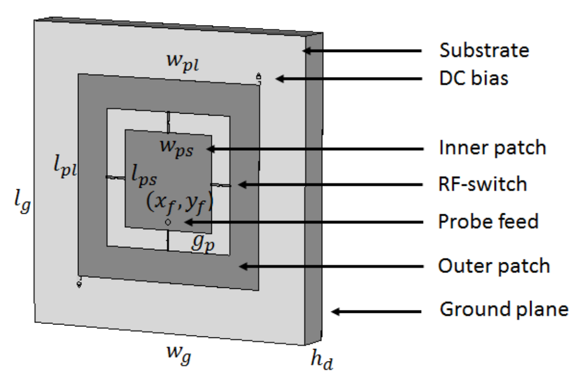

Fig. 1. The basic geometry of the reconfigurable L/S-band antenna element. Geometrical characteristics of the structure: w_{ps}= l_{ps}= 24mm, w_{pl}= l_{pl}= 50mm, l_g= w_g= 75mm, h_d= 9.144mm, g_p= 5mm, x_f= 0mm, y_f= -10 mm.

Manuscript received Mar 10, 2016; revised May 11, 2016.
N. Haider is with the Netherlands Organization of Applied Scientific Research (TNO, Defense, Security and Safety), 2597 AK Den Haag, The Netherlands (e-mail: nadia.haider@tno.nl).
A. G. Yarovoy and A. G. Roederer are with Delft University of Technology, Microwave Sensing, Signals and Systems (MS3), 2628 CD Delft, The Netherlands.

demonstrator and the measured results. Finally the concluding remarks are provided in Section IV.

II. THE L/S-BAND FREQUENCY RECONFIGURABLE ELEMENT

A. The Reconfigurable Element Concept

Reconfigurable antennas allow to modify the relevant circuital characteristics and/or radiation properties in real time. The implementation of several functionalities on the same antenna requires topological reconfigurability. The shape and size of the antenna should be adapted to the requirements set by the considered functionality. To design a frequency-reconfigurable phased array element, a new concept is investigated in this section.

Fig. 1 shows the geometry of the structure. A dual-patch is used to switch between L- and S-band. Reconfigurability is realized by controlling the RF switches to change the electrical size of the structure. When switches are in CLOSED state, the outer metal ring is connected to the inner patch and the antenna radiates in the lower band. When the switches are in OPEN state, the metal ring is detached from the inner patch and it acts as a parasitic element. Then, antenna operation in the higher band is achieved. As the main application of the array is thought to be radar, simultaneous operation of the array in both bands either in transmit or in receive modes is not considered.

The antenna is modeled on RO4003C substrate with permittivity ε_r=3.5. Its thickness has been set to λ_{dh}/6, where λ_{dh} is the wavelength in the dielectric at the highest frequency. The width and the length of the inner patch are 24 mm while those of the outer patch are 50 mm. Both radiating structures are symmetric along the principal planes ($w_{ps}= l_{ps}$ and $w_{pl}= l_{pl}$). This design approach provides dual polarization potential by inserting a second feeding probe.

The gap between the patches (g_p in Fig. 1) also affects performance. A large gap increases the deformation of the L-band patch from its conventional structure while a small one increases the parasitic effect of the outer ring at S-band. The ring acts as a parasitic structure at S-band and weakly radiates. The amount and the frequency of this unwanted radiation are directly influenced by the gap (g_p) between the patches. The gap width was set to 5 mm which shifted the parasitic radiation outside the radar L-band (1.2 – 1.4 GHz).

For the reconfigurable element design a probe feed is used. Here, probe feeding is more suitable than an indirect EM coupled feed, such as proximity- and aperture-coupled feed. The probe feed can be directly used for both feeding the antenna at radio frequency (RF) and controlling the DC-bias voltage for the switches.

The position of the feeding probe directly influences the input-impedance and, for the dual-band antenna, it is critical to provide an adequate match for each band. For the proposed design, it optimized to be x_f = 0 mm, y_f = -10 mm..

B. The Radio frequency (RF) Switch Implementation

RF switches, such as micro electro-mechanical systems (MEMS), varactors and p-I-n diodes [1-13], are often used in reconfigurable antennas. These technologies are well suited for antennas in printed technology. Switches, such as p-I-n diodes and RF MEMS, can electrically connect/disconnect metallic parts to introduce (discretized) changes in the geometry of the radiating surface. Taking into account the reliability, switching speed, power handling capability, lifetime and physical size, the p-I-n diode switches were selected for the considered reconfigurable radiating element.

The most important performance parameters for p-I-n diodes are isolation, insertion loss, power handling, switching speed and maximum frequency. The size and the package type of the components are also important and, considering these parameters, the GaAs beamlead p-I-n diode MA4AGBLP912 from MA-COM was selected for the antenna prototype. The thermal resistance of GaAs is generally higher than for silicon and hence the maximum power dissipation is less than for silicon material. However, a GaAs p-I-n diode provides much faster switching speed and less parasitic capacitance which makes it more suitable above 2 GHz.

The maximum power handling capability of the GaAs p-I-n diode (MA4AGBLP912) is 200mW and four diodes are connected in parallel in each antenna element. Therefore, the demonstrator is suitable for a maximum field strength of about 700V/m. The proposed antenna is primarily designed for digital beamforming on receive for which the power handling capability of the GaAs diode is sufficient. Furthermore, the proposed concept is an interesting solution for dual-band applications where the transmitted power is not extremely high, such as SATCOM and FMCW radar.

For digital beamforming on transmit the total transmitted power is high. For such radar systems with very high maximum incident power requirement the GaAs p-I-n diodes can be replaced by silicon diodes. Silicon diodes are usually suitable for incident power of few Watts. However, the higher parasitic values of silicon diodes need to be considered.

The third-order-intercept (IP3) and the 1-dB compression point of the MA4AGBLP912 diode occurs above 35 dBm and 25 dBm, respectively. Therefore, a fairly linear behavior of the diode can be expected within the intended power range. The number of the switching devices within the radiating structure also plays an important role and it must be limited for minimum cost and complexity. However, larger number of switches will increase system redundancy and thus also the reliability. For the concept demonstration four diode switches were used.

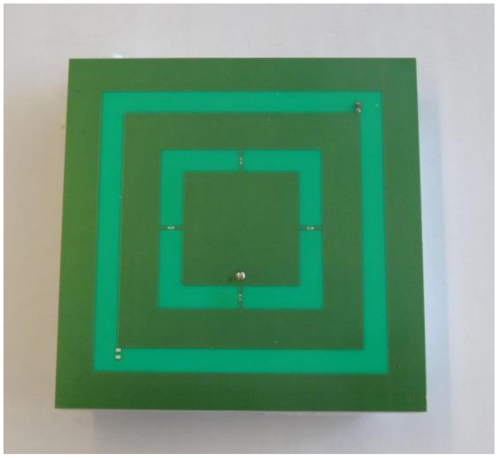

(a)

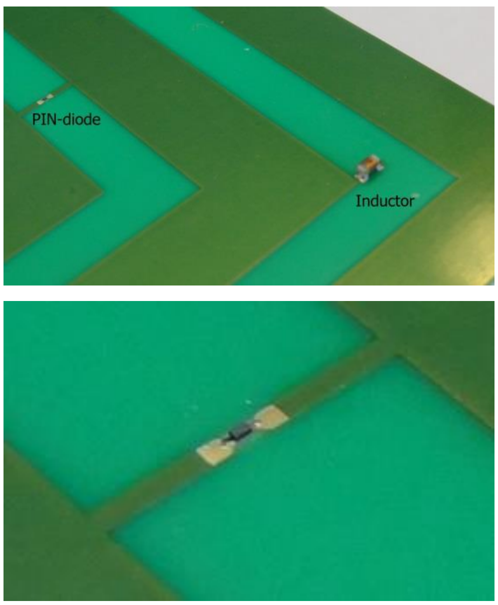

(b)

Fig. 2. (a) The L/S-band reconfigurable antenna prototype and (b) the p-I-n diode and the inductor attached on top of the radiating antenna

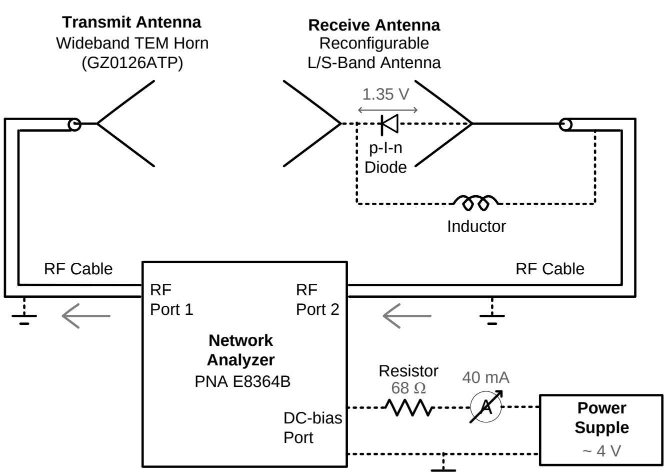

Fig. 3. The measurement scheme

The implementation of the DC bias circuit is challenging since these elements are designed for array application. Phased arrays usually contain thousands of radiating elements and placing additional lines in the antenna plane will drastically complicate the overall biasing network. To reduce such complexity, the DC control voltage was applied to the RF feed through a bias tee. DC ground was provided to the four p-I-n diodes using a single lumped inductor. A plated-through hole then connects this inductor to the back ground plane. The relevant SPICE-like equivalent circuit of the inductor was included in the antenna model to analyze the impact of the packaging and parasitic effects of the device.

C. The Experimental Verification

In order to verify the theoretical results, prototypes were designed and fabricated (Fig. 2). The measurement scheme is presented in Fig. 3.

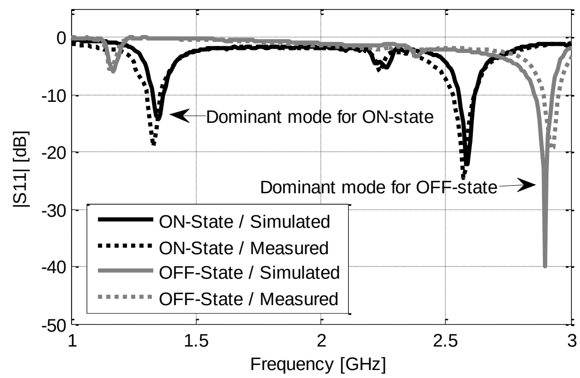

Fig. 4. Magnitude of the input-reflection coefficient

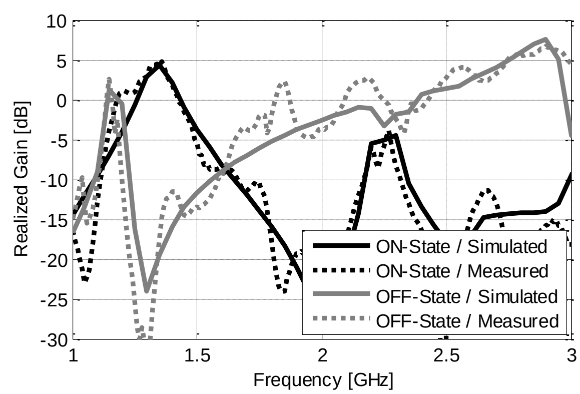

Fig. 5. Boresight realized gain as a function of frequency

Fig. 4 shows the magnitude of input-reflection coefficient for the ON and OFF states. Experimental results and theoretical predictions closely agree. In the diode ON-state, the antenna resonates at 1.33 GHz while it resonates at 2.95 GHz in the OFF-state. At L-band and at S-band the measured bandwidths (at -10 dB reflection level) are 60 MHz and 70 MHz, respectively. These narrow instantaneous bandwidths are helpful to protect the receivers against power jamming. In addition, operational frequency tuning within the radar bands is foreseen by proper matching of the reference impedance. This concept of frequency tuning by input-impedance tunable RF-frontend is discussed in [29-30].

Radiation measurements were carried out with a TEM horn (GZ0126ATP) as transmit antenna. In Fig. 5 the measured and simulated boresight realized gains are plotted. Here we notice good out-of-band gain suppression while maintaining adequate in-band gain. The measured peak gain is 4.7 dB at 1.36 GHz in the diode ON-state while it is 6.1 dB at 2.95 GHz for OFF-state. The gain remains above 3 dB from 1.3 GHz to 1.38 GHz and from 2.5 GHz to 3.05 GHz for the ON-state and OFF-state, respectively.

In the S-band diode OFF-state, the outer ring performs as a parasitic element causing a spurious resonance in the lower band. In the proposed design this undesired resonance was shifted below 1.2 GHz. Fig. 5 demonstrates that the spurious resonance due to the outer ring occurs around 1.15 GHz (outside the radar L-band). The measured results confirmed 23 dB and 24 dB isolations between the bands at 1.35 GHz and 2.95 GHz, respectively.

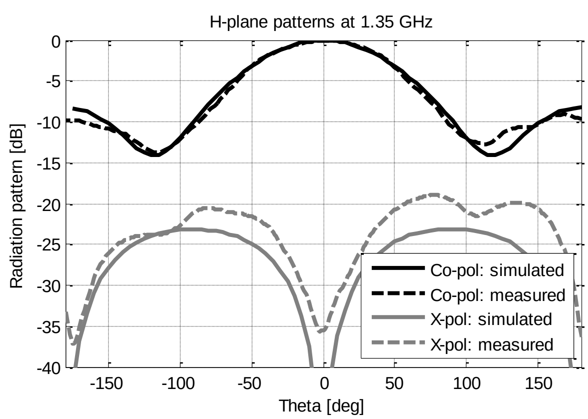

(a)

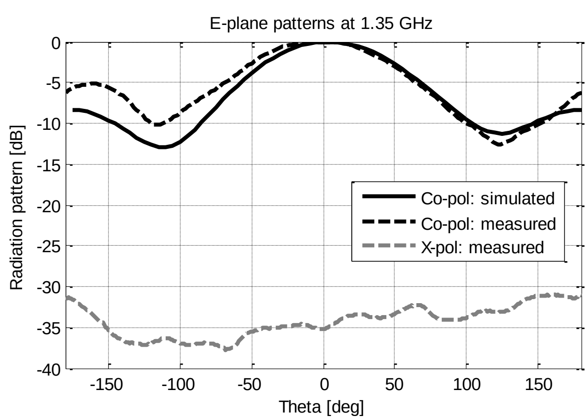

(b)

Fig. 6. Normalized radiation patterns for diode ON-state along (a) the H-plane (b) E-plane

Fig. 6 and Fig. 7 show the antenna radiation patterns in the E and H planes. At L-band, the half-power-beam-width (HPBW) is over 100° in both planes (Fig. 6). The measured cross-polar isolation in the scanning area (±60°) is over 25 dB in the E-plane. In the H-plane the polarization purity is reduced, but remains higher than 15 dB in the scan volume

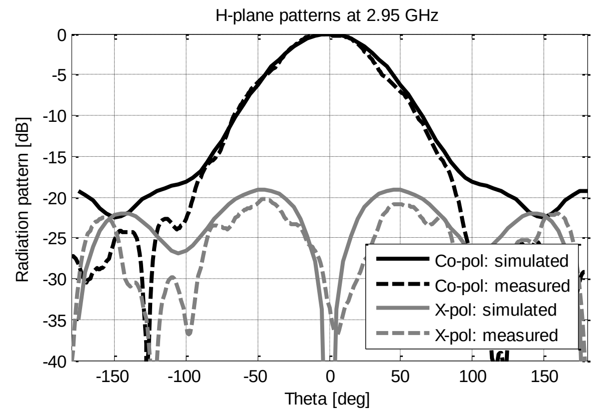

(a)

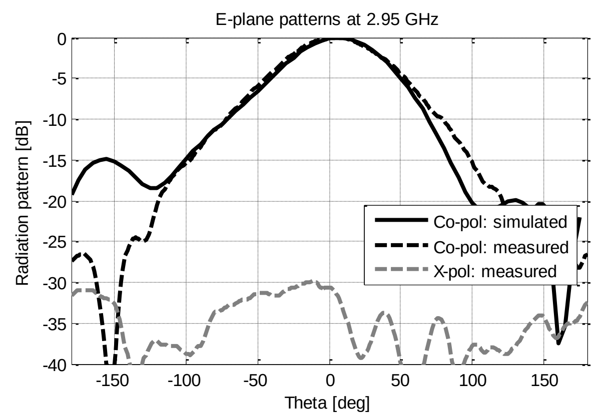

(b)

Fig. 7. Normalized radiation patterns for diode OFF-state along (a) the H-plane (b) E-plane

At S-band, the half-power-beam-width (HPBW) is about 70° in both principal planes (Fig. 7). In the E-plane, the element shows low cross-polarization as expected. The measured cross-polarization isolations remain more than 13 dB within the scanning area (±60°). In addition, the measured results verify a symmetric radiation pattern in the H-plane and a quasi-symmetric pattern in the E-plane for both modes.

In the proposed antenna topology the RF power directly passes through the diodes during the ON-state of the switches resulting in additional RF power losses. To experimentally verify the power loss by propagation through the p-I-n diodes in the ON-state, a second version of antenna has been made where the diodes where replaced by metal connections. Power loss was then evaluated by comparing the received power levels of the antenna using metal connections and using diodes. Within the operational band of the antenna the power loss due to the diodes varies between 1 and 1.7 dB (Fig. 8a) The total antenna efficiency (including mismatch losses) at L-band is about 60-70% (Fig, 8b) and the power loss caused by the diodes is the limiting factor here while at S-band it is about 80% (Fig. 8c). By using a switch with lower insertion loss one can overcome this limitation. Besides to equalize (if needed) the antenna array gains in the operational bands, the total apertures

This is the author's version of an article that has been published in this journal. Changes were made to this version by the publisher prior to publication.
The final version of record is available at http://dx.doi.org/10.1109/TAP.2017.2722685

for L-band array and S-band array might be different, e.g., the total aperture of L-band array might be larger than S-band one.

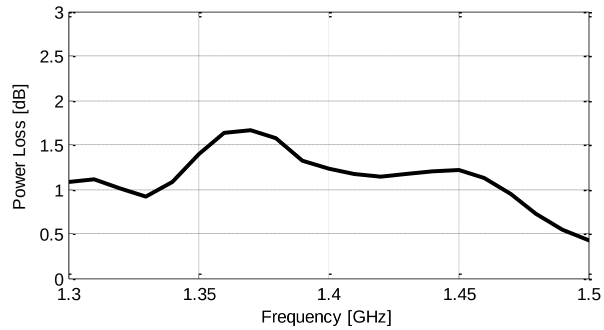

(a)

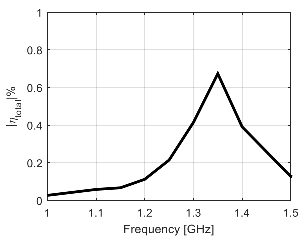

(b)

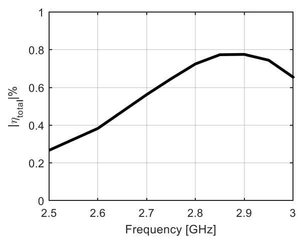

(c)

Fig. 8. (a) Measured power loss caused by the switching components (p-I-n diodes) of the reconfigurable antenna during ON-state and the total efficiency of the antenna element for (b) L-band mode and (c) S-band mode.

III. THE MULTI-SCALE ANTENNA ARRAY

In the previous section the L/S-band frequency reconfigurable isolated radiating element was presented. This section details the multi-scale array topology using such elements and providing large scanning capability in both frequency bands.

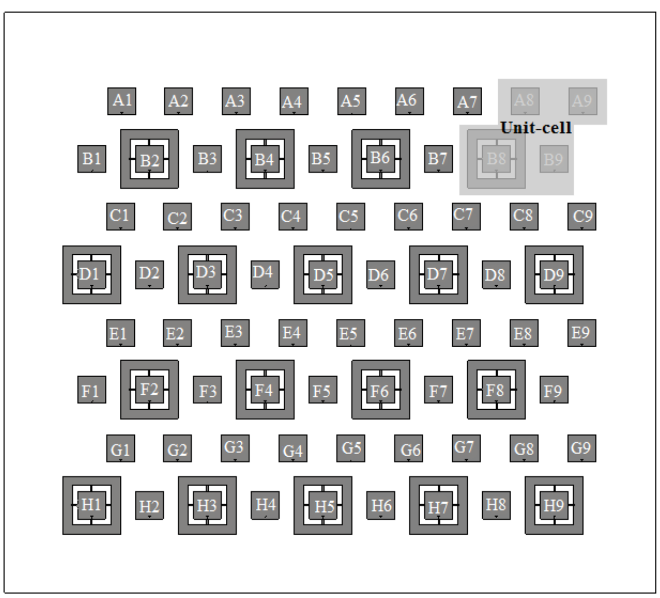

Fig. 9. The 9x8 multi-scale array structure for the experimental verification. At L-band only reconfigurable elements - At S-band all elements are excited

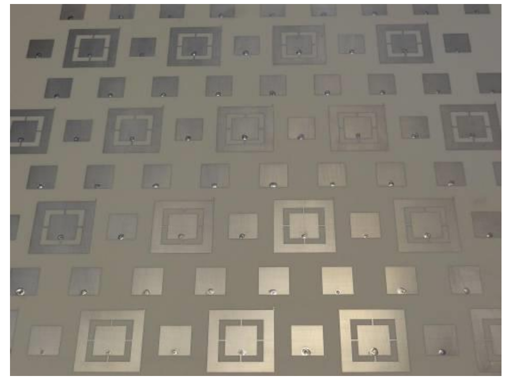

(a)

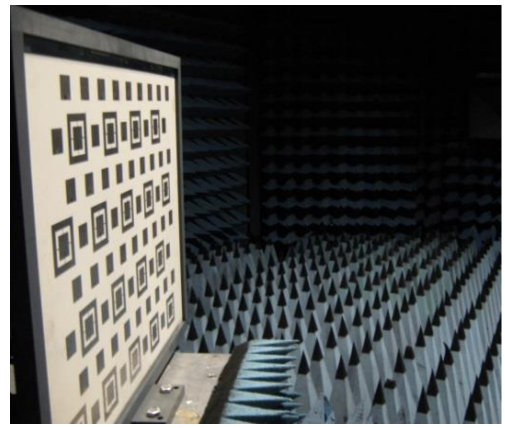

(b)

Fig. 10. (a) The multi-scale antenna array demonstrator, (b) The AUT placed inside the anechoic chamber

For a dense array with a regular grid one has to make a compromise between the maximum scan volume for the higher frequency band and the coupling level in the lower band. This limitation can be avoided by using a multi-scale array configuration. As illustrated in Fig. 9, each unit cell of this array will have one reconfigurable dual band element and three high frequency elements. For L-band, only recon-figurable elements are excited, while for S-band all the elements are used.

This array uses an equilateral triangular grid for each operational mode. The distance between two S-band elements is selected to be 50 mm and consequently, it is 100 mm between two L-band elements. This way, the inter-element spacing at both S-band and L-band becomes less than half of the free-space wavelength.

An array demonstrator of 72 elements was designed and measured. Fig. 9 shows the numerical model of this 9x8 array. Photographs of the prototype are shown in Fig. 10. Its size is 56.5 x 45.7 cm.

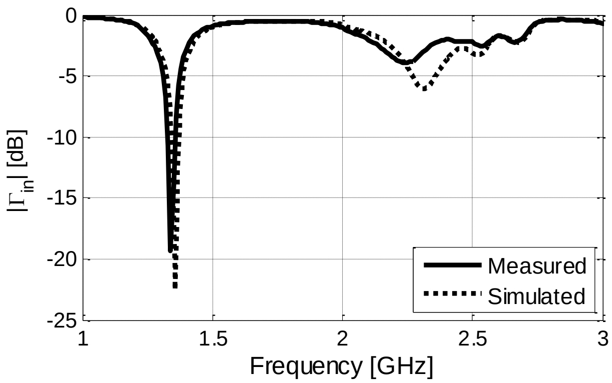

Fig. 11. The embedded input reflection coefficient of the centre element (D5 in Fig. 9) for L-band operation.

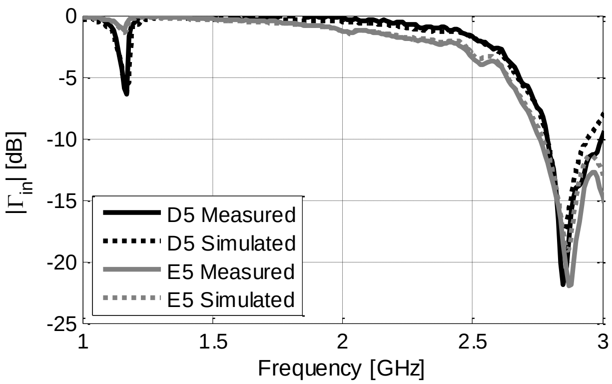

Fig. 12. The embedded input reflection coefficient of the centre elements (D5 and E5 in Fig. 9) for S-band operation.

A. The Reflection Coefficients

The input reflection coefficients of the embedded antenna elements in the finite 9x8 array were numerically investigated and verified with measurement. The embedded reflection coefficients of the center element (D5 in Fig. 9) at L-band are shown in Fig. 11. At S-band, the reflection coefficients of both the center reconfigurable element (D5 in Fig. 9) and the center S-band element (E5 in Fig. 9) are evaluated and presented in Fig. 12. The measured results are in good agreements with the simulated ones.

Fig. 13 and Fig. 14 show the measured active reflection coefficients of the center element for the L-band and S-band operations, which remain below -8 dB over about 50 MHz and 100 MHz, respectively. Here, the elements are sequentially excited to measure the embedded reflection and coupling coefficients (with loads on non-excited elements) and combined to synthesize the active reflection coefficients. If further improvement of the matching condition is desired, scan dependent input-impedance matching can be applied. Detailed discussion on this concept can be found in [29].

B. The Mutual Coupling Levels

Fig. 15 and Fig. 16 show the measured mutual couplings of the center element with three nearest ones. At L-band and S-band, the coupling along the H-planes remains below -12 dB and -15 dB within the respective bands (see Fig. 15 (a) and Fig.

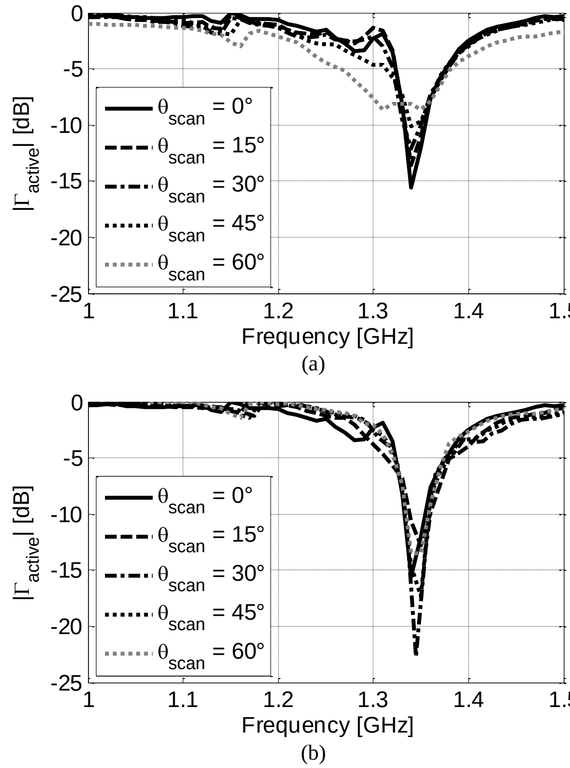

Fig. 13. The measured active reflection coefficients of the antenna within the finite array for the L-band operation. The scan angle varies along (a) the E-plane and (b) the H-plane.

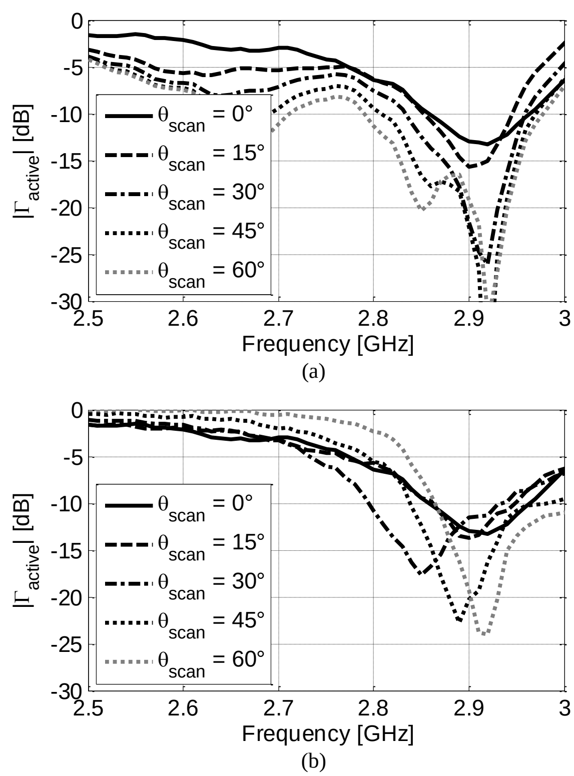

Fig. 14. The measured active reflection coefficients of the antenna within the finite array for the S-band operation. The scan angle varies along (a) the E-plane and (b) the H-plane.

This is the author's version of an article that has been published in this journal. Changes were made to this version by the publisher prior to publication.
The final version of record is available at http://dx.doi.org/10.1109/TAP.2017.2722685

16 (a)). Moreover, due to the triangular spacing the coupling remains well below -25 dB among elements in the diagonal planes (Fig. 15 (b) and Fig. 16 (b)). Thanks to these adequate isolations, expensive via cavities are avoided.

C. *The Scanning Performance*

For the investigations of the scanning performances, measured embedded element patterns are combined to synthesize the array radiation patterns. The embedded element pattern is measured with loads on non-excited elements [30]. In this case, the superposition of measured embedded realized gains provides an exact evaluation of the actual array patterns and scanning performance, assuming that T/R modules and feed network are matched to the nominal impedance used (here 50 Ohms). For the lower band, embedded radiation patterns of 16 elements are used, while 30 are used for the higher one. In Fig. 17 the measured embedded radiation patterns (H-plane) of the center element are shown. The cross-polarization suppression is higher than 10 dB within the scan range. Due to the relatively small size of the array the pattern differs for each element as presented in Fig. 18. The average peak realized gains are 4.9 dB and 5.6 dB while the half power beamwidths (HPBW) are about 110° and 100° and for L-band and S-band mode, respectively. Note that the array prototype is measured without actual diodes, meaning the diode losses are not included here.

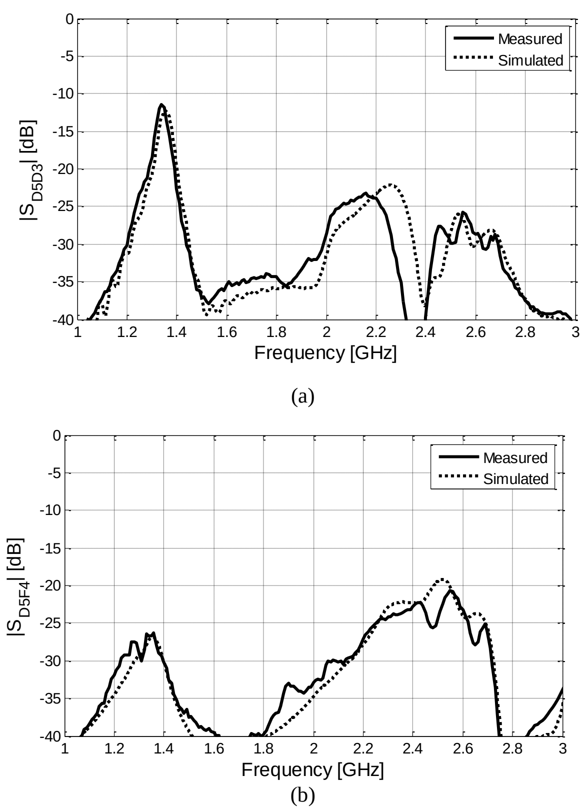

Fig. 15. The coupling coefficient of the centre element (D5 in Fig. 9) with (a) D3 and (b) F4 for L-band operation.

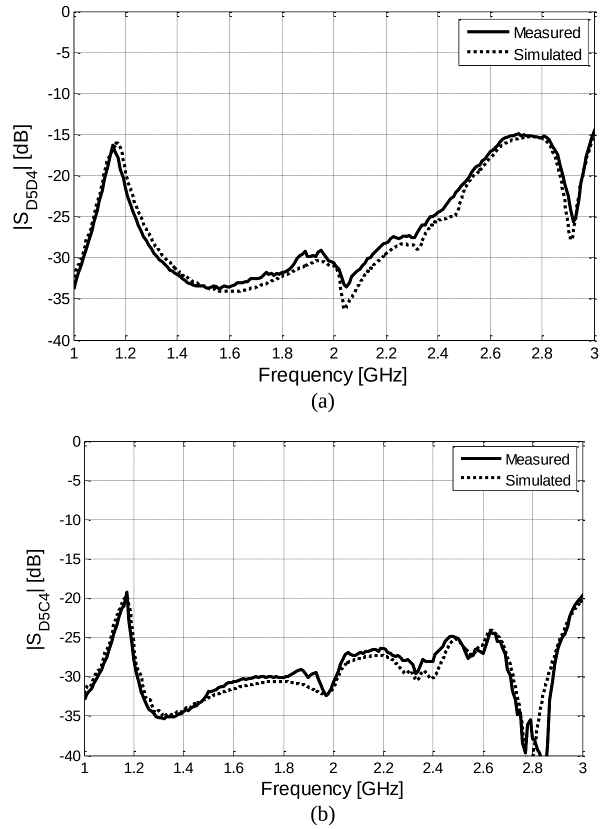

Fig. 16. The coupling coefficient of the centre element (D5 in Fig. 9) with (a) D4 and (b) C4 during S-band operation.

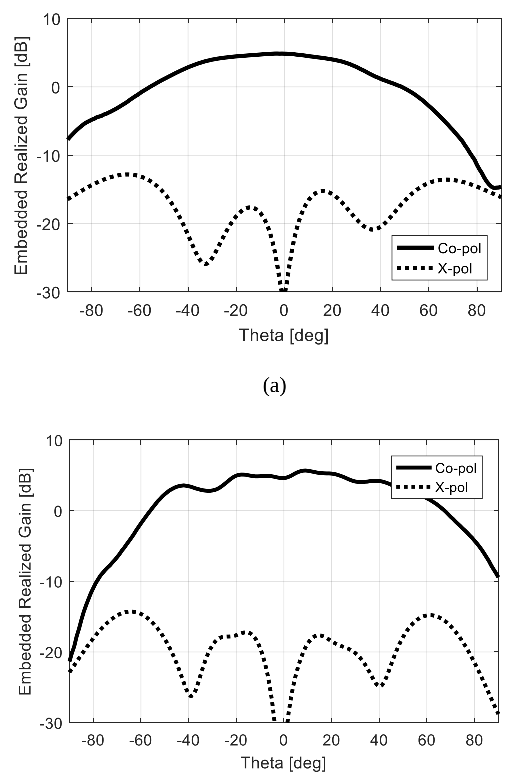

(b)

Fig. 17. Measured H-plane embedded realized gain for (a) L-band mode and (b) S-band mode

This is the author's version of an article that has been published in this journal. Changes were made to this version by the publisher prior to publication.
The final version of record is available at http://dx.doi.org/10.1109/TAP.2017.2722685

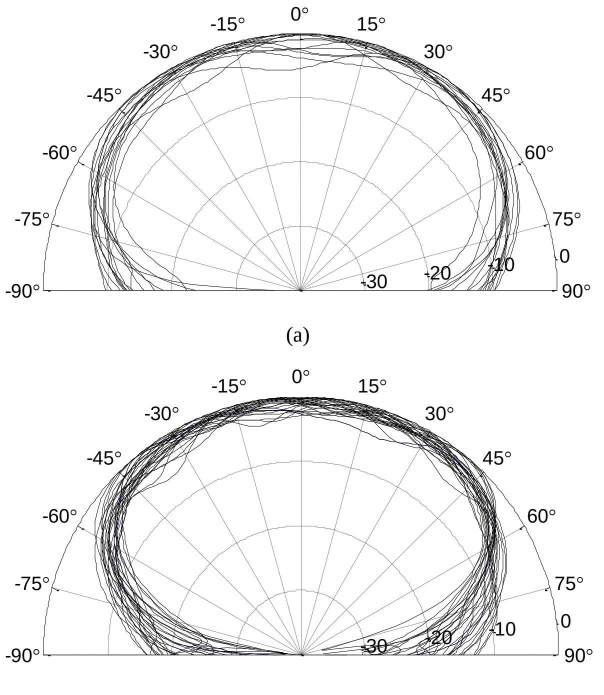

(a)

(b)

Fig. 18. Measured H-plane embedded element patterns for (a) the L-band (16 elements) and (b) the S-band (30 elements) operational modes

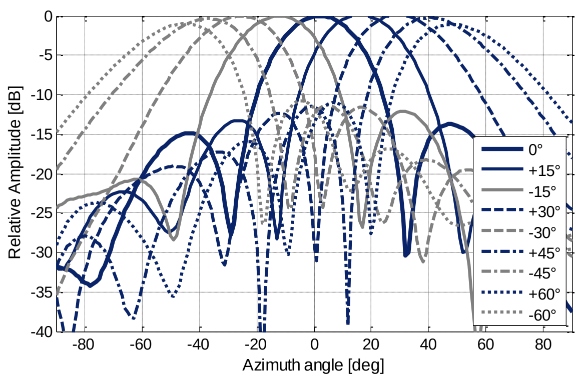

Fig. 19. Computed from the measured H-plane scan patterns at 1.35 GHz for 16 radiating elements

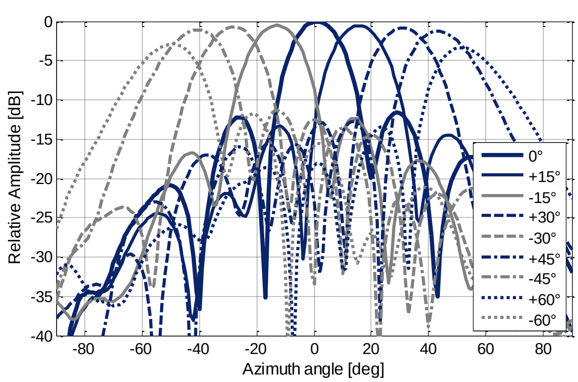

Fig. 20. Computed from the measured H-plane scan patterns at 2.95 GHz for 30 radiating elements

The H-plane scan patterns (computed from the measured embedded element patterns) are shown in Fig. 19 and Fig. 20 for L-band and S-band modes, respectively. Here, linear phase and uniform amplitude distributions are considered for the beam forming. As expected with spacings below a half wavelength, no grating lobes are present

In the proposed design, low scan loss is evident as shown in Fig. 19 and Fig. 20. The measured results verified that in the H-plane (beam steering up to ±60°) the variation in the relative amplitudes of the scan patterns remains below 3 dB and 5 dB at L-band and S-band, respectively. The sidelobe level remains 14 dB below the mainlobe for broadside scan and 10 dB for ±60° scan. Fig. 21 and Fig. 22 show good agreements between theoretical and experimental scan patterns at 2.95 GHz. Fig. 23 and Fig. 24 show simulated scan patterns in the E-plane for the L- and S-band modes, respectively.

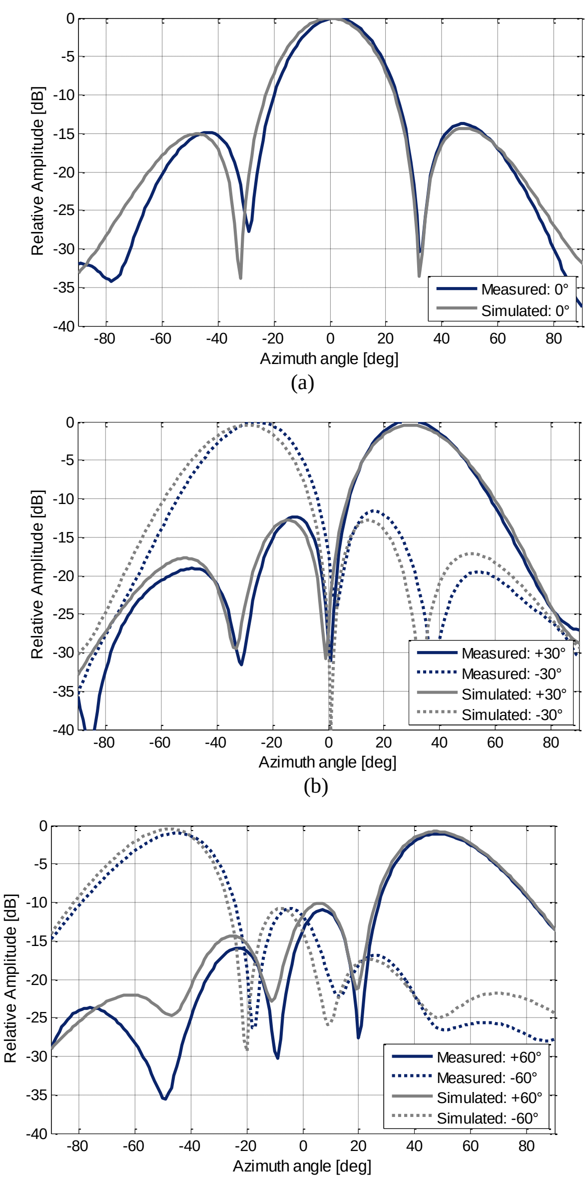

(a)

(b)

(c)

Fig. 21. Comparison between measured and simulated H-plane patterns at 1.35 GHz for 16 radiating elements, (a) 0° scan, (b) ±30° scan, (c) ±60° scan

This is the author's version of an article that has been published in this journal. Changes were made to this version by the publisher prior to publication.
The final version of record is available at http://dx.doi.org/10.1109/TAP.2017.2722685

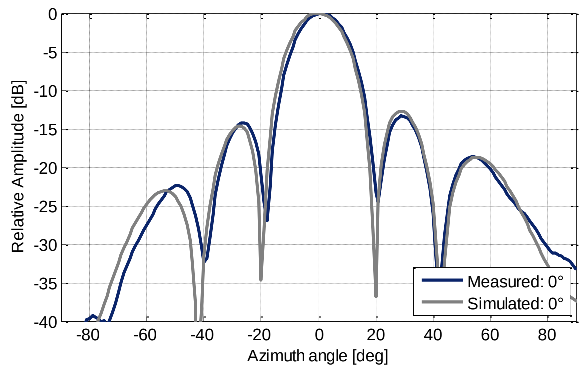

(a)

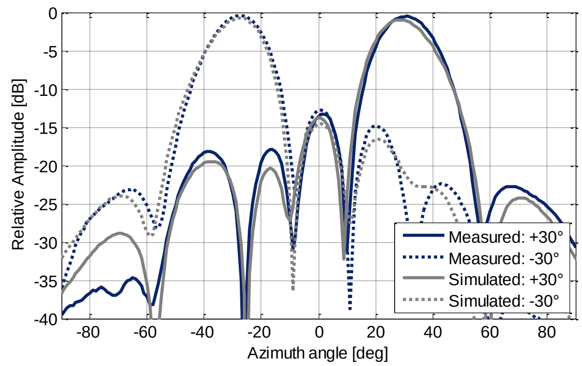

(b)

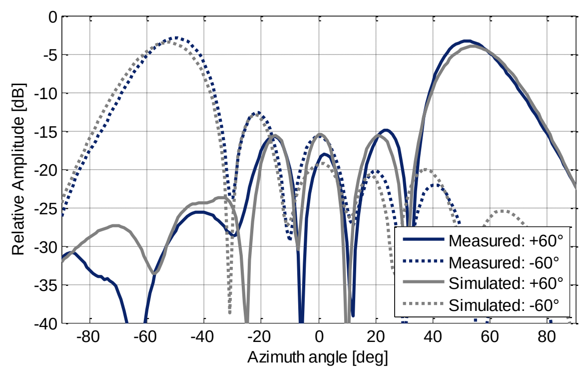

(c)

Fig. 22. Comparison between measured and simulated H-plane patterns at 2.95 GHz for 30 radiating elements, (a) 0° scan, (b) ±30° scan, (c) ±60° scan

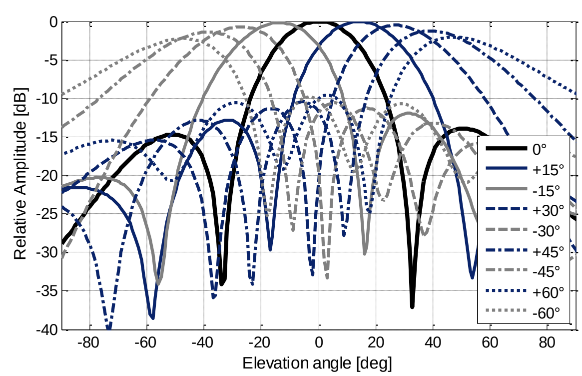

Fig. 23. E-plane simulated scan patterns at 1.35 GHz for 16 radiating elements

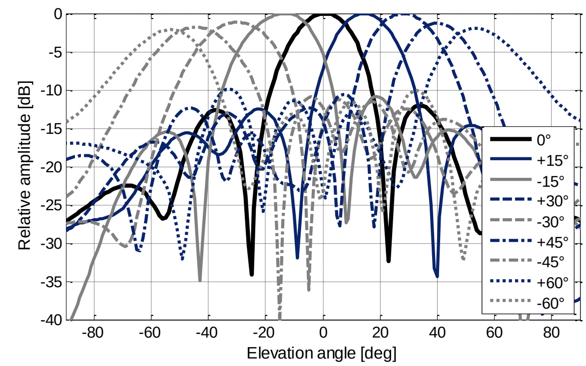

Fig. 24. E-plane simulated scan patterns at 2.95 GHz for 30 radiating elements

IV. CONCLUSION

This article details the concept and the realization of a frequency reconfigurable phased array antenna based on modifying the element aperture. The change of the electrical size of the antenna element was achieved by altering the state of the p-I-n diode switches placed on the radiating structure. The experimental verifications confirmed that the proposed concept is applicable to frequency switch between L and S radar bands with a frequency separation of 2.2:1. The antenna concept also includes a versatile biasing circuit for array configuration. In the proposed design the complexity of the bias network was considerably reduced by controlling the DC bias voltage level through the RF feed. The element has compact size of 50 x 50 mm² which makes it attractive for phased array application with large scanning volume in both bands. The measured results verified 5 to 6 dB realized-gains with about 20 dB isolations between the bands. One of the limiting factors the power loss in the switches. In this work a p-I-n diode with low insertion loss was selected which resulted in a moderate level of power loss ranging between 1.0 and 1.7 dB in the band for the CLOSED state of the switches.

The novel multi-scale array architecture was implemented to avoid the limitations of a dual-band dense arrays to achieve simultaneously good radiation efficiency in the L-band and wide grating lobe free scanning region for the S-band. With the multi-scale array configuration, half a wavelength inter-element spacing was maintained for both L-band and S-band. This reduced the coupling levels in L-band. Consequently, the radiation efficiency and scanning capabilities in this band are improved. For the S-band, the reduced element spacing of the multi-scale array architecture increased the maximum scan angle to ±60° while in the dense array arrangement it would be limited to ±25°. A planar 9x8 multi-scale array demonstrator was designed and the measured results closely matched the numerical predictions.

ACKNOWLEDGMENT

This research is conducted as part of the Sensor Technology Applied in Reconfigurable systems for sustainable Security (STARS) project. For further information: www.starsproject.nl. The authors wish to thank Thales Nederland for their help in antenna array measurement, Diego Caratelli for many useful discussions, Johan Zijderveld and Pascal Aubry for their support during the antenna measurements and the reviewers for their helpful comments and suggestions. PCLL (Printech Circuit Laboratories Ltd) is acknowledged for its help in the antenna prototype fabrication.

REFERENCES

[1] C. R. White and G. M. Rebeiz, "Single- and dual-polarized tunable slot-ring antennas," *IEEE Trans. on Antennas and Propagat.*, vol. 57, no. 1, pp. 19-26, 2009.

[2] Y. Tawk, J. Costantine, and C. G. Christodoulou, "A varactor based reconfigurable filtenna," *IEEE Antennas and Wireless Propagation Letters*, vol. 11, pp. 716–719, 2012.

[3] S. L. S. Yang, A. A. Kishk, and F. L. Kai, "Frequency reconfigurable U-slot microstrip patch antenna," *IEEE Antennas Wireless Propag. Lett.*, vol. 7, pp. 127–129, May 2008.

[4] K. R. Boyle and P. G. Steeneken, "A five-band reconfigurable PIFA for mobile phones," *IEEE Trans. on Antennas and Propagat.*, vol. 55, no. 11, pp. 3300–3309, 2007.

[5] A. Vasylchenko, X. Rottenberg, B. X. Broze, M. Nuytemans,W. De Raedt, and G. A. E. Vandenbosch, "A frequency switchable antenna based on MEMS technology," in *Proceedings of the 4th European Conference on Antennas and Propagation* (EuCAP '10), pp. 1–3, April 2010.

[6] A. Grau, J. Romeu, M. J. Lee, S. Blanch, L. Jofre, and F. De Flaviis, "A Dual-Linearly-polarized MEMS-reconfigurable antenna for narrowband MIMO communication systems," *IEEE Trans. on Antennas and Propagat.*, vol. 58, no. 1, pp. 4–17, 2010.

[7] C.-Y. Chiu, J. Li, S. Song, and R. D. Murch, "Frequency reconfigurable pixel slot antenna," *IEEE Trans. on Antennas and Propagat.*, vol. 60, no. 10, pp. 4921–4924, 2012.

[8] S. V. Hum and H. Y. Xiong, "Analysis and design of a differentially-fed frequency agile microstrip patch antenna," *IEEE Trans. on Antennas and Propagat.*, vol. 58, no. 10, pp. 3122–3130, 2010.

[9] M. R. Hamid, P. Gardner, P. S. Hall, and F. Ghanem, "Switched band Vivaldi antenna," *IEEE Trans. on Antennas and Propagat.*, vol. 59, no. 5, pp. 1472–1480, 2011.

[10] T.-Y. Han and C.-T. Huang, "Reconfigurable monopolar patch antenna," *Electronics Letters*, vol. 46, no. 3, pp. 199–200, 2010.

[11] D. Peroulis, K. Sarabandi, and L. P. B. Katehi, "Design of reconfigurable slot antennas," *IEEE Trans. on Antennas and Propagat.*, vol. 53, no. 2, pp. 645–654, 2005.

[12] M. Martınez-Vazquez, O. Litschke, M. Geissler, D. Heberling, A. M. Martınez-Gonzalez, and D. Sanchez-Hernandez, "Integrated planar multiband antennas for personal communication handsets," *IEEE Trans. on Antennas and Propagat.*, vol. 54, no. 2, pp. 384–391, 2006.

[13] A. Grau, J. Romeu, M. J. Lee, S. Blanch, L. Jofre, and F. De Flaviis, "A Dual-Linearly-polarized MEMS-reconfigurable antenna for narrowband MIMO communication systems," *IEEE Trans. on Antennas and Propagat.*, vol. 58, no. 1, pp. 4–17, 2010.

[14] C. R. Liu, S. Q. Xiao, Y. X. Guo, Y. Y. Bai, and B. Z. Wang, "Broad-band circularly polarized beam-steering antenna array," *IEEE Trans. Antennas Propag.*, vol. 61, no. 3, pp. 1475–1479, Mar. 2013.

[15] A. Thain, G. Peres, A. Hulzinga, H. Schippers, and H. Van Gemeren, "A dual-band low profile phased array antenna for civil aviation applications," in *Proceedings of the 3rd European Conference on Antennas and Propagation*, Berlin, Mar. 2009.

[16] K. Lee, A. T. S. Wang, and R. S. Chu, "A dual band phased array using interleaved waveguides and dipoles printed on high dielectric substrate," in *Proceedings of the IEEE AP-S Symp.*, vol. 2, pp. 886–889, Jun. 1984.

[17] O. H. Karabey, S. Bildik, C. Fritzsch, S. Strunck, A. Gaebler, R. Jakoby, and A. Manabe, "Liquid crystal based reconfigurable antenna," in *Proceedings of the 32th ESA Antenna Workshop on Antennas for Space Applications*, Noordwijk, The Netherlands, 2010.

[18] M. A. Soliman, T. E. Taha, W. Swelam, and A. Gomaa, "3.5/5GHz dual-band 8x8 adaptive array antenna," *Progress In Electromagnetics Research C*, Vol. 34, pp. 85-98, 2013.

[19] L. Shafai, W. Chamma, M. Barakat, P. Strickland, and G. Seguin, "Dual-band dual-polarized perforated microstrip antennas for SAR applications," *IEEE Trans. Antennas Propag.*, vol. 48, no. 1, pp. 58–66, Jan. 2000.

[20] D. Isleifson and L. Shafai, "A Study on the Design of Dual-Band Perforated Microstrip Antennas for SAR Applications," *International Symposium on Antenna Technology and Applied Electromagnetics (ANTEM)*, Toulouse, Jun. 2012.

[21] E. Arnieri, L. Boccia, and G. Amendola, "A Ka-Band Dual-Frequency Radiator for Array Applications," *IEEE Antennas and Wireless Propagat. Letters*, vol. 8, Aug. 2009.

[22] Z. Sun, K. P. Esselle1, S.-S. Zhong, and Y. J. Guo, "Shared-Aperture Dual-Band Dual-Polarization Array Using Sandwiched Stacked Patch," *Progress In Electromagnetics Research C*, vol. 52, 183–195, Aug. 2014.

[23] S.-S. Zhong, Z. Sun, L.-B. Kong, C. Gao, W. Wang, and M.-P. Jin, "Tri-Band Dual-Polarization Shared-Aperture Microstrip Array for SAR Applications" *IEEE Trans. on Antennas and Propagat.*, vol. 60, no. 9, pp. 4157–4165, Sep. 2012.

[24] K. Naishadham, R. L. Li, L. Yang, T. Wu, W. Hunsicker, and M. Tentzeris, "A shared-aperture dual-band planar array with self-similar printed folded dipoles," *IEEE Trans. on Antennas Propag.*, vol. 61, no. 2, pp. 606–613, Feb. 2013.

[25] L. Infante, A. De Luca and M. Teglia, "Low-profile ultra-wide band antenna array element suitable for wide scan angle and modular subarray architecture," *Phased Array Systems and Technology (ARRAY), 2010 IEEE International Symposium on*, pp. 157-163, Waltham, MA, 2010.

[26] J. P. Doane, K. Sertel and J. L. Volakis, "A Wideband, Wide Scanning Tightly Coupled Dipole Array With Integrated Balun (TCDA-IB)," in *IEEE Transactions on Antennas and Propagation*, vol. 61, no. 9, pp. 4538-4548, Sep. 2013.

[27] D. Cavallo, A. Neto, G. Gerini, A. Micco and V. Galdi, "A 3- to 5-GHz Wideband Array of Connected Dipoles With Low Cross Polarization and Wide-Scan Capability," in *IEEE Transactions on Antennas and Propagation*, vol. 61, no. 3, pp. 1148-1154, Mar. 2013.

[28] N. Haider, D. P. Tran, A. G. Roederer, and A. G. Yarovoy, "Reconfigurable L/S band phased array," *Electronics Letters*, vol. 47, no. 23, pp. 1265 - 1266, Nov. 2011.

[29] N. Haider, D. Caratelli, and A. G. Yarovoy, "Frequency Reconfiguration of a Dual-Band Phased-Array Antenna with Variable-Impedance Matching," *IEEE Transactions on Antennas and Propagation,* vol. 63,no. 8, pp. 3477- 3485, June 2015.

[30] P. Kildal, S. Maci, A. Vosoogh, "Fundamental Directivity Limitations of Dense Array Antennas: A Numerical Study Using Hannan´s Embedded Element Efficiency," in *IEEE Antennas and Wireless Propagation Letters*, vol. PP, Aug. 2015.

Nadia Haider received the M.Sc. (*cum laude*) and Ph.D. degrees in electrical engineering from Delft University of Technology, Delft, the Netherlands, in 2010 and 2015, respectively. From 2009 to 2014, she was with the Microwave Sensing, Systems and Signals Group, Delft University of Technology.
In 2015, she joined Netherlands Organization for Applied Scientific Research (TNO), The Netherlands, as a Scientist. Since 2016, she has been also a lead applied EM scientist at Qu-tech (a collaboration founded by TU Delft and TNO). Her research interests include full-wave analysis and design of passive devices and antennas for radar, satellite and wireless applications, active phased arrays, impedance matching, reconfigurable technologies and electromagnetic analysis and the design of quantum bits and quantum circuits.

Alexander G. Yarovoy graduated from the Kharkov State University, Ukraine, in 1984 with the Diploma with honor in radiophysics and electronics. He received the Candidate Phys. & Math. Sci. and Doctor Phys. & Math. Sci. degrees in radiophysics in 1987 and 1994, respectively.
In 1987 he joined the Department of Radiophysics at the Kharkov State University as a Researcher and became a Professor there in 1997. From September 1994 through 1996 he was with Technical University of Ilmenau, Germany as a Visiting Researcher. Since 1999 he is with the Delft University of Technology, the Netherlands. Since 2009 he leads there a chair of

Microwave Sensing, Systems and Signals. His main research interests are in ultra-wideband microwave technology and its applications (in particular, radars) and applied electromagnetics (in particular, UWB antennas). He has authored and co-authored more than 250 scientific or technical papers, four patents and fourteen book chapters. He served as a Guest Editor of five special issues of the IEEE Transactions and other journals. Since 2011 he is an Associated Editor of the International Journal of Microwave and Wireless Technologies.

Prof. Yarovoy is the recipient of the European Microwave Week Radar Award for the paper that best advances the state-of-the-art in radar technology in 2001 (together with L.P. Ligthart and P. van Genderen) and in 2012 (together with T. Savelyev). In 2010 together with D. Caratelli Prof. Yarovoy got the best paper award of the Applied Computational Electromagnetic Society (ACES).

Prof. Yarovoy served as the Chair and TPC chair of the 5th European Radar Conference (EuRAD'08), Amsterdam, the Netherlands, as well as the Secretary of the 1st European Radar Conference (EuRAD'04), Amsterdam, the Netherlands. Prof. Yarovoy served also as the co-chair and TPC chair of the Xth International Conference on GPR (GPR2004) in Delft, the Netherlands. Since 2008 he serves as Director of the European Microwave Association (EuMA).

Antoine Roederer was born near Paris in 1943. He received the BSEE degree from l' Ecole Supérieure d' Electricité, Paris, in 1964, the MSEE degree at the University of California, Berkeley, with a Fulbright Fellowship, in 1965 and the Doctorate of Electrical Engineering (honors) from Université de Paris VI, in 1972. He joined ESRO (now ESA) in 1973 where he initiated and supervised for many years R&D and project support for space antennas. In 1993, he became Head of the Electromagnetics Division. His interests include innovation and development in the field of antennas. Prior to joining ESA, he first designed broadcast antennas at JAMPRO in Sacramento (1967). He then served in the French Army Research (1968), taught electromagnetics at the ESME Engineering School in Paris and was radar antenna R&D engineer with THOMSON-CSF (1968-1973). He was European representative of the IEEE Antenna and Propagation Society, where he has held several functions, including IEEE Distinguished Lecturer in 1995-1996. He has also been active in the British IEE and in the French SEE. He has been Chairman of the EU COST 260 Project on Smart Antennas. He was the initiator and chairman of the Millennium Conference on Antennas and Propagation, AP 2000 in Davos, precursor of the large EUCAP conferences.

He was one of the founders and advisors of the EU Network of Excellence on Antennas, ACE. He has authored or co-authored over 150 papers, several book chapters, and holds 20 patents in the field of antennas. This has included aspects of wideband communications, broadcasting, radar and satellite antennas, with emphasis on log-periodics, reflectarrays, multiple beam reflectors and arrays and advanced antenna feed networks. Dr Roederer received numerous awards for his contributions to the field of antennas and to the antenna community in Europe. Among these the Ampère Award from the French SEE, the European Space Agency Inventor Award, a Doctorate Honoris Causa from the Technical University of Delft, the Award of the European Association on Antenna and Propagation, the British Roderick James Lifetime Achievement Award. He is Life Fellow of the IEEE. Dr Roederer retired from ESA in 2008.

He is now part time scientific advisor at the Technical University of Delft. He is also consultant on multiple beam antennas and gives lectures on advanced feed networks. He was married to Judith N. Harris († 2004) and has three Children: Emilie, Etienne and Thomas.